FULL PAPER

ADVANCED FUNCTIONAL MATERIALS

# Size- and Shape-Control of Crystalline Zinc Oxide Nanoparticles: A New Organometallic Synthetic Method

By *Myrtil L. Kahn*,* *Miguel Monge*, *Vincent Collière*, *François Senocq*, *André Maisonnat*, and *Bruno Chaudret**

A novel organometallic synthetic method has been developed for the preparation of crystalline ZnO nanoparticles of controlled size and shape. Isotropic nanoparticles with a mean size between 3 and 6 nm and nanorods with a mean diameter of 3–4 nm and length up to 120 nm have been obtained in this way. This synthetic method takes advantage of the exothermic reaction of the precursor $Zn(c\text{-}C_6H_{11})_2$ (**1**) toward moisture and air and involves the presence of long-alkyl-chain amines as stabilizing ligands. The influence of the different experimental parameters (concentration, solvent, nature of the ligand, time, and temperature) on the size and shape of the ZnO nanoparticles has been studied, together with the mechanism of their formation, by NMR spectroscopy, transmission electron microscopy, and X-ray diffraction techniques. The nanoparticles prepared in this way can be dissolved in most of the common organic solvents, forming colloidal solutions. The surface state of the nanoparticles as well as the possibility of forming luminescent solutions from which regular monolayers can be deposited are also reported.

## 1. Introduction

Zinc oxide is a material of particular interest because it possesses unique optical and electronic properties. It is a wide-bandgap semiconductor (3.37 eV) that is also luminescent, and has emerged as a good candidate for many applications. This interest in ZnO has stimulated research in a wide range of domains. For example, thin films of ZnO have been reported to display good conductivity and high transparency in the visible region, and have been envisaged as transparent electrodes for solar cells.[1] Zinc oxide nanoparticles have also been investigated as gas sensors[2] and materials for electrodes,[3] and, recently, an ultraviolet lasing effect has been observed at room temperature using ZnO nanowires.[4] These fascinating examples are based on the control of both the physical and chemical properties of the nanoparticles, which depend on several factors, namely the particle size and size dispersity, the shape of the particles, the surface state, the crystal structure, the organization of the particles onto a support, and their dispensability. It is well known that these factors depend on the synthetic method used and, as a consequence, applications of nanomaterials are directly linked to the successful control of the synthetic process.

Various different physical or chemical synthetic approaches have been developed. Several reports on physical ZnO syntheses have been published. They involve, for example, vapor-phase oxidation,[5] thermal vapor transport and condensation (TVTC),[6,7] and chemical vapor deposition (CVD)[8] methods. However, for these approaches to give crystalline particles they must be performed at high temperature (500–1500 °C). On the other hand, chemical methods are of particular interest since they offer the potential of facile scale-up and take place at moderate temperature (100–200 °C). Among these chemical methods, precipitation,[9–11] sol–gel,[12–14] and microemulsion[15] approaches are convenient and may lead to nanomaterials of controlled morphology. However, these syntheses make use of ionic species which may interact with the growth process of the particle and hence modify the final material.[16] For example, the nature of the ions present in solution can influence processes such as coarsening and aggregation, which can compete with nucleation and growth leading to a modification of the particle size distribution, as reported by Hu et al.[16] Organometallic complexes have been used to overcome this problem. For example, $Zn(C_2H_5)_2$ has been reported to be a good precursor for ZnO after its transformation into an alkoxide prior to hydrolysis and heat treatment.[17] This precursor has also been used for the synthesis of ZnO following a "high-temperature organometallic method" derived from that originally reported by Bawendi and co-workers.[18]

Several years ago we initiated a research project aimed at the preparation of either metal[19–26] or metal-oxide nanoparticles,[27–30] with organometallic complexes as precursors. Our approach consists in the synthesis of the metal nanoparticles by taking advantage of the reactivity of organometallic precursors toward gases such as $H_2$ or CO, or, alternatively, by UV irradiation or heat treatment. Following this method, we have demonstrated that the size and shape of metal nanoparticles can be controlled by the ligands present in solution. Metal-oxide nanoparticles have been prepared in a similar way but using a two-

[*] Dr. M. L. Kahn, Dr. B. Chaudret, Dr. M. Monge, V. Collière, Dr. A. Maisonnat
Laboratoire de Chimie de Coordination, CNRS UPR 8241
205 route de Narbonne, 31077 Toulouse Cedex 04 (France)
E-mail: mkahn@lcc-toulouse.fr; chaudret@lcc-toulouse.fr
Dr. F. Senocq
CIRIMAT, UMR CNRS 5085, ENSIACET
118, Route de Narbonne, 31077 Toulouse Cedex 04 (France)

[**] This research was supported by the Centre National de la Recherche Scientifique, CNRS. The authors thank J. F. Meunier for TGA measurements. M.M. thanks the Spanish M.E.C.D. (Fellowship: EX2002-0319) for financial support. Supporting Information is available from Wiley InterScience (http://www.wileyinterscience.com) or from the author.

  DOI: 10.1002/adfm.200400113 

ADVANCED FUNCTIONAL MATERIALS



step approach where metal nanoparticles are synthesized in the first step and oxidized in a controllable manner in the second step. This approach has allowed the preparation of $SnO_2$[30] and $In_2O_3$[29] particles and has also been used for the preparation of ZnO[28] particles from the dialkylzinc precursor $Zn(c\text{-}C_6H_{11})_2$ ($c\text{-}C_6H_{11}$ = cyclohexyl; **1**). However, we reasoned that most organometallic complexes are air-sensitive and decompose exothermically in air. We also supposed that the kinetics of this decomposition may control the formation of the nanomaterial. Therefore a controlled oxidation of the precursor in solution could lead, in one step, to oxide nanoparticles, the shape and size of which could be controlled by the different parameters of the system (such as the nature of the organometallic precursor, the ligands or surfactants present, the solvent used, and so on).

We report in this paper a one-pot, room-temperature, organometallic synthetic method for the preparation of ZnO nanoparticles of controlled size and shape. A preliminary communication of part of these results has already been published.[31] The influence of the different experimental parameters on the size and shape of the ZnO nanoparticles, as well as the mechanism of their formation, have been studied and are reported here. The surface state of the nanoparticles and the possibility to form luminescent solutions from which regular monolayers can be deposited are also reported. This synthetic method has the advantage that it is very easy to perform and leads to quantitative yields of ZnO nanoparticles. These two points are of particular importance given the interest for such a nanomaterial in basic research and also for potential applications in various domains such as in micro- and optoelectronics.

## 2. Results

### 2.1. Synthesis

In order to test the potential of the method for the direct preparation of oxide nanoparticles from organometallic precursors, we first studied the decomposition of the organometallic precursor in solution in the absence of added ligands. For example, when a tetrahydrofuran (THF) solution of the dicyclohexylzinc(II) complex **1** is left to stand at room temperature (RT) in air, the solvent slowly evaporates and leaves a white and luminescent residue characterized by X-ray diffraction (XRD) and transmission electron microscopy (TEM) as agglomerated ZnO nanoparticles with a zincite structure displaying no defined size or shape (Coll1; Table 1 and Fig. 1a). Similar results were obtained when other solvents were used, such as toluene (Coll2), pentane (Coll3), or diethyl ether (Coll4; Supporting Information, Fig. S1). These results demonstrated the ease of access to zinc oxide, but it was then of interest to try to control the growth of the particles by introduction of ligands into the reaction mixture.

If ligands such as long-alkyl-chain amines were added, well-defined nano-objects were formed, the size and shape of which depend upon the reaction conditions. For example, under our "standard conditions", complex **1** was dissolved in THF under argon in the presence of hexadecylamine (HDA; [**1**]/[HDA] = 1:1; concentration of reagents: 0.042 mol $L^{-1}$) and the solution was allowed to stand under argon for 17 h. Subsequent slow evaporation of the solvent in air over four days led to the formation of homogeneous nanorods of about 8.1 nm × 2.6 nm (Coll5; Fig. 1b). Several parameters were identified as important for controlling the size, shape, and homogeneity of the nanoparticles, namely the nature of the ligands, the relative concentration of reagents, the solvent, the overall concentration of reagents, the reaction time, the evaporation time, and the reaction/evaporation temperature. These parameters and their influence on the ZnO nano-objects are listed in Tables 2,3.

**Table 1.** Agglomerated ZnO particles prepared in the absence of ligand.

| Coll n° | Ligand (per $ZnCy_2$) | Solvent | Time [a] | Overall concentration | Temp | Size [nm] | Morphology |
|---|---|---|---|---|---|---|---|
| Coll1 | – | THF | 17 hours/4 days | 0.042 M | RT | – | Agglomerated nanoparticles |
| Coll2 | – | toluene | 17 hours/4 days | 0.042 M | RT | – | Agglomerated nanoparticles |
| Coll3 | – | pentane | 17 hours/4 days | 0.042 M | RT | – | Agglomerated nanoparticles |
| Coll4 | – | diethyl ether | 17 hours/4 days | 0.042 M | RT | – | Agglomerated nanoparticles |

[a] The first value corresponds to the incubation time whereas the second one corresponds to the time in moisture and air.

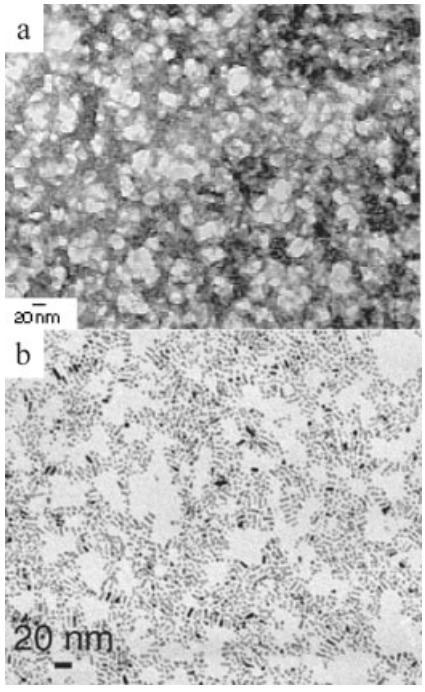


**Figure 1.** a) Agglomerated nanoparticles of ZnO with a zincite structure, displaying no defined size or shape, obtained by direct exposure of a THF solution of **1** to air and b) ZnO nanoparticles obtained using the standard conditions.

  

**Table 2.** Nanoparticles prepared in the presence of a ligand and a solvent.

| Coll n° | Ligand (per $ZnCy_2$) | Solvent | Time [a] | Overall concentration | Temp | Size [b] [nm] | Morphology |
|---|---|---|---|---|---|---|---|
| Coll5 | HDA | THF | 17 hours/4 days | 0.042 M | RT | 8.1 ± 3.3 × 2.6 ± 0.8 nm | Nanorods |
| Coll6 | DDA | THF | 17 hours/4 days | 0.042 M | RT | 3.0 ± 1.1 nm | Nanoparticles |
| Coll7 | OA | THF | 17 hours/4 days | 0.042 M | RT | 4.0 ± 1.5 nm | Nanoparticles |
| Coll11 | HDA | Toluene | 17 hours/4 days | 0.042 M | RT | 4.6 ± 1.8 nm | Nanoparticles |
| Coll12 | HDA | Heptane | 17 hours/4 days | 0.042 M | RT | 2.4 ± 1.1 nm | Nanoparticles |
| Coll13 | HDA | Anisole | 17 hours/4 days | 0.042 M | RT | 3.0 ± 1.2 nm | Nanoparticles |
| Coll14 | HDA | Diethyl ether | 17 hours/4 days | 0.042 M | RT | 3.7 ± 1.2 nm | Nanoparticles |
| Coll15 | DDA | Toluene | 17 hours/4 days | 0.042 M | RT | 5.5 ± 1.6 nm | Nanoparticles |
| Coll16 | DDA | Heptane | 17 hours/4 days | 0.042 M | RT | 4.3 ± 2.0 nm | Nanoparticles |
| Coll17 | DDA | Anisole | 17 hours/4 days | 0.042 M | RT | 3.7 ± 1.2 nm | Nanoparticles |
| Coll18 | DDA | Diethyl ether | 17 hours/4 days | 0.042 M | RT | 3.6 ± 1.9 nm | Nanoparticles |
| Coll19 | OA | Toluene | 17 hours/4 days | 0.042 M | RT | 5.7 ± 3.2 nm | Nanoparticles |
| Coll20 | OA | Heptane | 17 hours/4 days | 0.042 M | RT | 3.5 ± 1.5 nm | Nanoparticles |
| Coll21 | OA | Anisole | 17 hours/4 days | 0.042 M | RT | 3.1 ± 1.7 nm | Nanoparticles |
| Coll22 | OA | Diethyl ether | 17 hours/4 days | 0.042 M | RT | 3.2 ± 1.2 nm | Nanoparticles |
| Coll23 | HDA | THF | 17 hours/4 days | 0.125 M | RT | 11.4 ± 5.7 × 2.8 ± 0.7 nm | Nanorods |
| Coll24 | HDA | THF | 17 hours/4 days | 0.250 M | RT | Mixture of disks and medium size rods | Nanorods |
| Coll25 | HDA | THF | 17 hours/4 days | 0.01 M | RT | < 3.0 nm after 1 day<br>4.3 ± 1.1 nm after 4 days | Nanoparticles |
| Coll29 | HDA | THF | 5 mins/4 days | 0.042 M | RT | 5.8 ± 2.7 × 2.7 ± 0.6 nm | Nanorods |
| Coll30 | HDA | THF | 2 weeks/4 days | 0.042 M | RT | 4.1 ± 1.7 nm | Nanoparticles |
| Col31 | HDA | THF | 17 hours/24 hours | 0.042 M | RT | 2.5 ± 0.6 nm | Nanoparticles |
| Coll32 | HDA | Toluene | 17 hours/24 hours | 0.042 M | RT | 4.1 ± 1.2 nm | Nanoparticles |
| Coll33 | HDA | Heptane | 17 hours/24 hours | 0.042 M | RT | 2.4 ± 1.6 nm | Nanoparticles |
| Coll34 | HDA | Anisole | 17 hours/24 hours | 0.042 M | RT | 2.4 ± 1.2 nm | Nanoparticles |
| Coll35 | DDA | THF | 17 hours/24 hours | 0.042 M | RT | 2.6 ± 1.1 nm | Nanoparticles |
| Coll36 | DDA | Toluene | 17 hours/24 hours | 0.042 M | RT | 4.3 ± 1.6 nm | Nanoparticles |
| Coll37 | DDA | Heptane | 17 hours/24 hours | 0.042 M | RT | 2.3 ± 0.6 nm | Nanoparticles |
| Coll38 | DDA | Anisole | 17 hours/24 hours | 0.042 M | RT | 3.0 ± 1.0 nm | Nanoparticles |
| Coll39 | OA | THF | 17 hours/24 hours | 0.042 M | RT | 2.3 ± 1.1 nm | Nanoparticles |
| Coll40 | OA | Toluene | 17 hours/24 hours | 0.042 M | RT | 3.1 ± 1.6 nm | Nanoparticles |
| Coll41 | OA | Heptane | 17 hours/24 hours | 0.042 M | RT | 2.6 ± 1.1 nm | Nanoparticles |
| Coll42 | OA | Anisole | 17 hours/24 hours | 0.042 M | RT | 3.1 ± 1.2 nm | Nanoparticles |
| Coll45 | HDA | THF | 17 hours/4 days | 0.042 M | 45 °C | 3.7 ± 1.6 nm (24 h)<br>4.8 ± 0.7 nm (4 days) | Nanoparticles |

[a] The first value corresponds to the incubation time whereas the second one corresponds to the time in moisture and air. [b] The mean diameter is evaluated by fitting of the histogram with a Gaussian curve. The first value corresponds to the center of the peak whereas the second one corresponds to twice the standard deviation of the Gaussian distribution or approximately 0.849 the width of the peak at half-height.

**Table 3.** Nanoparticles prepared in the presence of a ligand without any other solvent.

| Coll n° | Ligand (per $ZnCy_2$) | Solvent | Time [a] | Overall concentration | Temp | Size [b] [nm] | Morphology |
|---|---|---|---|---|---|---|---|
| Coll8 | HDA | No | 17 hours/4 days | – | RT | 10.7 ± 3.7 × 1.6 ± 0.7 nm | Nanorods |
| Coll9 | DDA | No | 17 hours/4 days | – | RT | 9.2 ± 4.0 × 3.7 ± 0.7 nm | Nanorods |
| Coll10 | OA | No | 17 hours/4 days | – | RT | 7.4 ± 2.7 × 2.8 ± 1.2 nm | Nanorods |
| Coll26 | 2 DDA | No | 17 hours/4 days | – | RT | 17.1 ± 3.4 × 3.0 ± 0.9 nm | Nanorods |
| Coll27 | 2 OA | No | 17 hours/4 days | – | RT | 2.8 ± 0.3 nm width (24h)<br>3.7 ± 0.3 nm width (4 days) | Nanorods 20–60 nm (24 h)<br>Nanorods 20–120 nm (4 days) |
| Coll28 | 5 OA | No | 17 hours/4 days | – | RT | 3.8 ± 1.3 nm width (24 h)<br>4.1 ± 1.4 nm width (4 days) | Nanorods 30–60 nm (24 h)<br>Nanorods 30–80 nm (4 days) |
| Coll43 | 2 OA | No | no/4 days | – | RT | 2.2 ± 0.3 nm width | Nanorods 30–120 nm (4 days) |
| Coll47 | HDA | No | 17 hours/4 days | – | 45 °C | Mixture | Nanoparticles + Nanorods |
| Coll48 | 2 OA | No/$O_2$ | 17 hours/4 days | – | RT | – | No particle |
| Coll49 | 2 OA | No/$H_2O$ | 17 hours/4 days | – | RT | | Nanorods |

[a] The first value corresponds to the incubation time whereas the second one corresponds to the time in moisture and air. [b] The mean diameter is evaluated by fitting of the histogram with a Gaussian curve. The first value corresponds to the center of the peak whereas the second one corresponds to twice the standard deviation of the Gaussian distribution or approximately 0.849 the width of the peak at half-height.

  

ADVANCED FUNCTIONAL MATERIALS



*2.1.1. Ligand Effects*

Addition of dodecyl amine (DDA) or octylamine (OA) instead of HDA under otherwise standard conditions led to spherical nanoparticles with a mean diameter of 3.0 (Coll6) or 4.0 nm (Coll7; Fig. 2a,b, respectively). The synthesis may also be performed in the presence of only **1** and the stabilizing ligand, in the absence of solvent. In such cases the solution is formed either by dissolution in the liquid ligand (OA) or by the reaction of **1** with the ligand to give a new complex, the melting point of which is below room temperature (for HDA and DDA, see the NMR spectroscopic study below). Thus, mixing equimolar amounts of **1** and an amine yielded nanorods of $10.7 \times 1.6$ (HDA, Coll8), $9.2 \times 3.7$ (DDA, Coll9), and 7.4 nm $\times$ 2.8 nm (OA, Coll10; Figs. 2c,d,e, respectively). Therefore, an increase in the length of the alkyl chain results in an increase of the shape anisotropy.

*2.1.2. Solvent Effects*

Using the standard conditions but replacing THF with other solvents such as toluene, (Coll11), heptane (Coll12), anisole (Coll13), or diethyl ether (Coll14) produced nanoparticles of isotropic morphology with a mean diameter of 4.6, 2.4, 3.0, and 3.7 nm, respectively (Fig. 3). It is also possible to vary both the solvent and the nature of the ligand at the same time. In this instance, using DDA and either toluene, heptane, anisole, or diethyl ether, spherical nanoparticles with a mean size of 5.5 (Coll15), 4.3 (Coll16), 3.7 (Coll17), and 3.6 nm (Coll18) were obtained, respectively, whereas using OA and the same solvents produced particles with mean sizes of 5.7 (Coll19), 3.5 (Coll20), 3.1 (Coll21), and 3.2 nm (Coll22), respectively (Supporting Information, Fig. S2). It therefore appears from this study that the influence of the nature of solvents on the size and shape of the particles is complex. Indeed, several parameters related to the solvent appear to be important for the control of the growth of the particles, namely its miscibility with water, its coordinating ability, and its evaporation rate. It is therefore not easy to draw definitive conclusions.

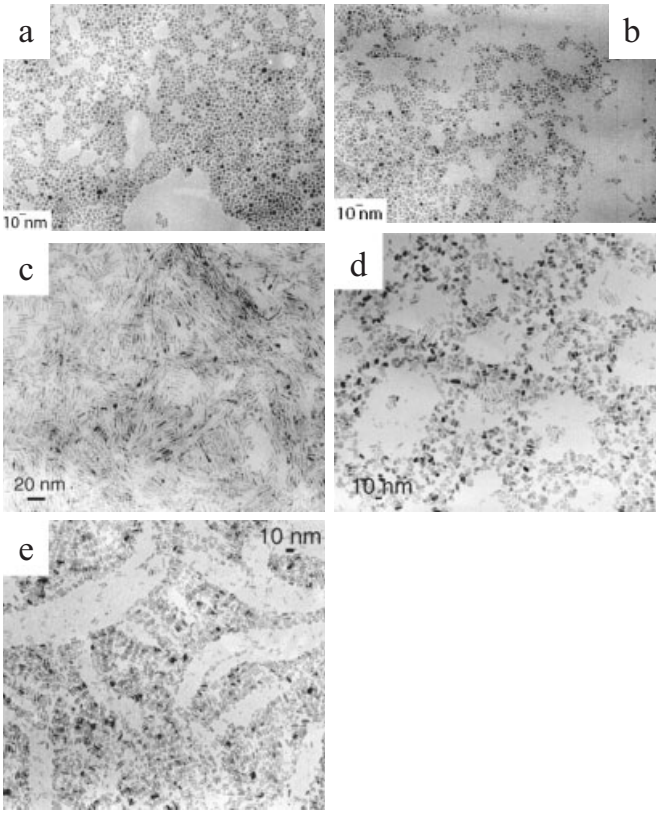


**Figure 2.** Ligand effects: a) standard conditions but replacing HDA with dodecylamine (DDA); b) standard conditions but replacing HDA with octylamine (OA); c) synthesis performed with HDA in the absence of other solvents; d) synthesis performed with DDA in the absence of other solvents; and e) synthesis performed with OA in the absence of other solvents.

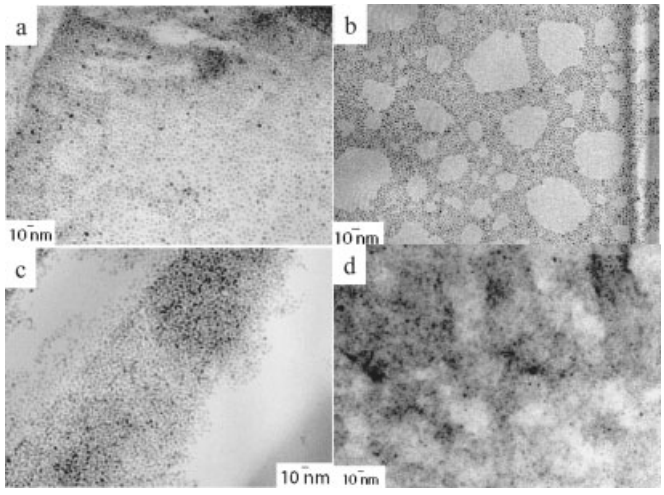


**Figure 3.** Solvent effects: synthesis performed under standard conditions but replacing THF with: a) toluene; b) heptane; c) anisole; and d) diethyl ether.

*2.1.3. Concentration Effects*

Nanorods of 11.4 nm $\times$ 2.8 nm were obtained under the standard conditions but increasing the overall concentration of reagents from 0.042 to 0.125 mol $L^{-1}$ (Coll23; Fig. 4a). The width of the nanoparticles is similar to that observed using the standard conditions but their length increases, leading to nano-objects with a higher aspect ratio. If the concentration of reagents is raised further to 0.250 mol $L^{-1}$, a mixture of spherical nanoparticles and nanorods was obtained (Coll24). A decrease of the concentration to 0.010 mol $L^{-1}$ led to spherical nanoparticles of about 4.3 nm (Coll25; Fig. 4b). Another important parameter is the concentration ratio between the zinc precursor and the ligand ([HDA]/[Zn]). For example, if this ratio is less than one inhomogeneous samples are obtained whatever the ligand. In contrast, for concentration ratios higher than one homogeneous samples are obtained, the size of which depends on the concentration ratio. For example, doubling the concentration of amine relative to zinc in the absence of solvent pro-

  

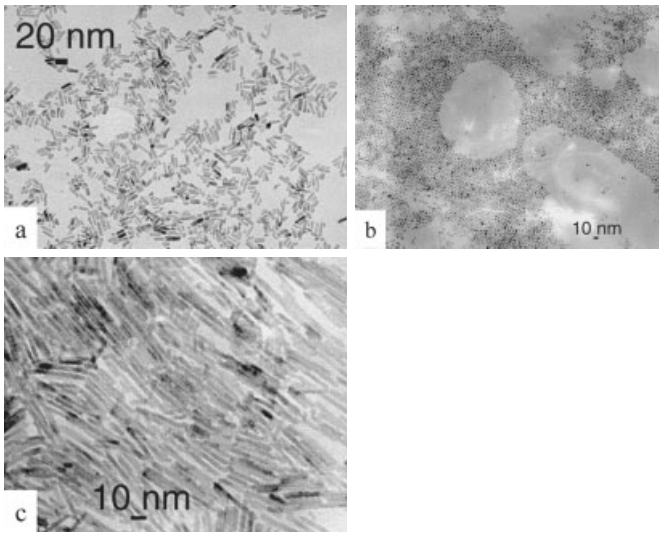


**Figure 4.** Concentration effects: synthesis performed under standard conditions but changing the overall concentration to: a) 0.125 mol $L^{-1}$; b) 0.01 mol $L^{-1}$; and c) synthesis performed with two equivalents of OA in the absence of other solvents.

duces nanorods of 17.1 nm × 3.0 nm for DDA (Coll26), and longer nanorods up to 120 nm (mean diameter of 2.8 nm) in the case of OA (Coll27; Fig. 4c). Increasing the concentration of OA (5 equiv) leads to nanorods with more homogeneous length (ranging from 30 to 80 nm) and a mean width of 4.1 nm (Coll28). It is therefore possible to increase the aspect ratio of the nanorods by playing with two parameters: the concentration of precursor and ligand and/or the concentration ratio between the ligand and the precursor. However, there is a limit for these parameters above which inhomogeneous samples are obtained. This point will be developed further in the Discussion section.

*2.1.4. Time Effects*

According to our synthetic procedure, two different time parameters have been studied. The first one is the time during which the solution is kept under an inert atmosphere before the beginning of the evaporation/oxidation process, which is the second time parameter. For example, if the reaction time under argon is cut to 5 min instead of 17 h, under otherwise standard conditions, shorter nanorods of about 5.8 nm × 2.7 nm are obtained (Coll29; Fig. 5a). Similarly, a slower oxidation/evaporation process (two weeks instead of four days) produces nanoparticles with a mean diameter of 4.1 nm (Coll30; Fig. 5b). For reactions performed in a solvent, however, if the oxidation/evaporation process is stopped after only 24 h very small spherical particles are obtained with a mean diameter of about 2.5 nm whatever the solvent and the ligand, except for the particles prepared in toluene, which have a mean diameter of about 4.0 nm (Coll31, Coll32, Coll33, and Coll34 for HDA; Coll35, Coll36, Coll37, and Coll38 for DDA; and Coll39, Coll40, Coll41, and Coll42 for OA in THF, toluene, heptane, and anisole, respectively; Fig. 5c and Supporting Information, Fig. S3.) In the absence of an incubation time nanorods are obtained in the presence of two equivalents of OA and in the absence of further solvent (Coll43; Fig. 5d). The effect of the oxidation time was also studied with two equivalents of OA in the absence of solvent (Coll44; Fig. 6). After 1 h spherical nanoparticles of 1.8 nm are observed, which transform into nanorods after 4 h (width of 2.1 nm). After that time, the width of the nanorods is apparently constant: it is 2.1 and 2.2 nm for 9 and 24 H of oxidation, respectively. The length of the nanorods ranges from 30 to 120 nm but the number of longer rods increases as the oxidation time increases. The effect of time will be discussed further in association with problems of nucleation

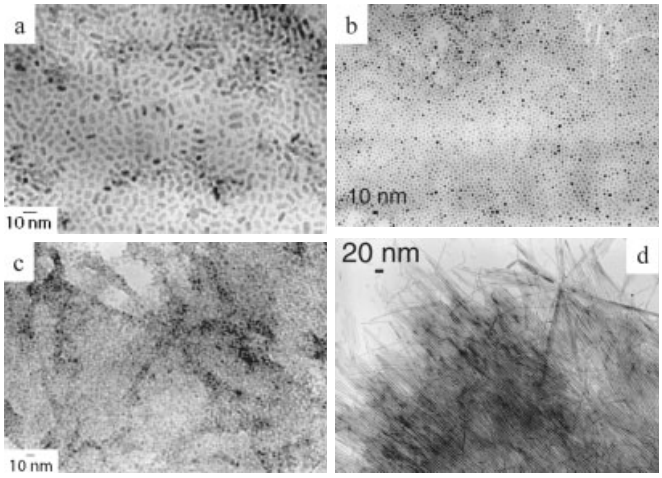


**Figure 5.** Time effects: synthesis performed under standard conditions but with: a) a reduction of the reaction time under argon to 5 min; b) a slow oxidation/evaporation process (two weeks instead of four days); c) oxidation/evaporation process stopped after only 24 h; and d) synthesis performed with two equivalents of OA without other solvent and without an incubation period.

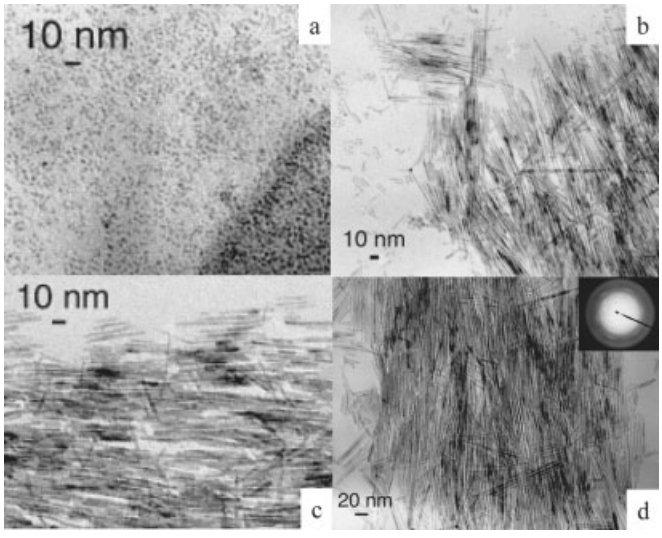


**Figure 6.** Evolution of size and shape as a function of time of the nanoparticles synthesized with one quivalent of OA in absence of other solvents: a) after 1 h of oxidation; b) after 4 h of oxidation; c) after 9 h of oxidation; and d) after 24 h of oxidation.

  

ADVANCED FUNCTIONAL MATERIALS



and growth. In addition, it should be noted that the nanorods tend to self-organize as evidenced by the selected-area electron diffraction (SAED) pattern (Fig. 6d, insert), which shows diffraction spots that are indicative of highly oriented nanorods.

*2.1.5. Temperature Effects*

Increasing the reaction temperature to 45 °C, under otherwise standard conditions, leads to nano-objects with an isotropic shape and a mean diameter of 4.8 nm (Coll45; Supporting Information, Fig. S4a). Similar results were obtained after incubation at room temperature and increase of the temperature to 45 °C during the oxidation period (Coll46; Supporting Information, Fig. S4b). However, inhomogeneous samples were obtained from reactions performed with amine ligands in the absence of solvents at a reaction temperature of 45 °C (Coll47). Consequently, the increase of temperature favors the formation of isotropic nano-objects in the presence of a solvent but leads to inhomogeneous samples in the absence of solvent. It is noteworthy that the increase of temperature involves an inherent increase of the evaporation rate of the solvent, which may also have an impact on the size and shape of the particles.

## 2.2. Characterization

*2.2.3. TEM Measurements*

All lengths, widths, and diameters of the particles were determined by TEM. Moreover, ultramicrotomy was performed to determine the thickness of the nano-objects. For example, ultramicrotomy performed on nanorods prepared in the absence of solvent with two equivalents of OA shows well-defined solid circles with diameters ranging from 2.5 to 3 nm, in good agreement with the measured mean width (Supporting Information, Fig. S5).

*2.2.4. X-Ray Measurements*

All XRD diagrams display the same pattern in the 15° to 40° $\theta$ range, which corresponds to the hexagonal zincite phase (space group $P6_3mc$). No crystalline hydroxide phase is observed. Additional peaks that vary as a function of the ligand used are observed at lower $\theta$ values (5–13° range); all samples prepared with the same ligand display similar additional peaks (Fig. 7). This observation may result from a long-range organization of the sample that may be induced by the ligands coordinated at the surface of the particles. Indeed, when the X-ray diffraction measurements were performed at different temperatures all additional peaks were removed at 300 °C and only the diffraction diagram of the hexagonal zincite phase of ZnO remained. Moreover, this assumption was strengthened by the NMR spectroscopic study (see below), which shows that the ligands remain at the surface of the particles.

When the shape of the nanoparticles corresponds to nanorods, the diffractograms present a narrow half-height width (full width at half maximum, FWHM) of the *002* diffraction line compared to the *100* and *101* diffraction peaks. In contrast, isotropic nanoparticles show no particular narrowness of the *002* diffraction line. Indeed, similar half-height widths are observed for the *002*, *100*, and *101* diffraction peaks. The small half-height width of the *002* diffraction line observed for the nanorods is in agreement with the existence of a privileged axis of growth—the *c* axis of the zincite phase for the ZnO nanorods. The size of the crystallite was estimated using the Debye–Scherrer equation. For example, according to the comparison between the *002* and the *100* diffraction peaks, an aspect ratio of 2.5 and 2.1 was found for nanorods synthesized using one equivalent of DDA and OA, respectively. These calculations suggest the presence of longer nanorods when using DDA, in good agreement with the TEM measurements. Similar results were obtained if the ratio was calculated using the *101* diffraction peak instead of *100*.

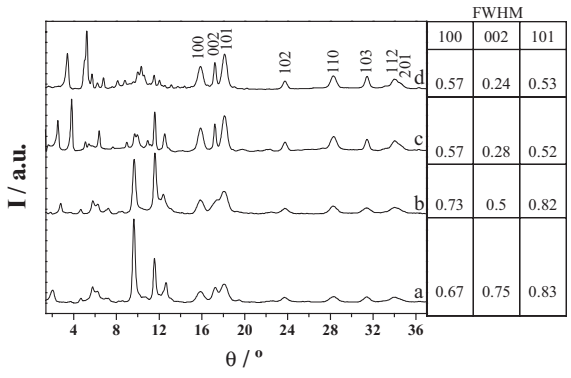


**Figure 7.** X-ray diffraction pattern recorded at room temperature for: a) the particles synthesized with HDA in $Et_2O$; b) the particles synthesized with HDA in toluene; c) the particles synthesized in DDA; and d) the particles synthesized in OA.

*2.2.5. NMR Spectroscopic Study*

$^1$H and $^{13}$C{$^1$H} NMR spectra were recorded to determine the role of the ligand during the synthetic process (before and after oxidation). Before oxidation, addition of HDA to **1** in $d^8$-THF leads to $^1$H NMR spectra suggesting the coordination of the amine to **1** through nitrogen. Indeed, the $^1$H NMR spectrum of free HDA shows a triplet signal at $\delta = 2.62$ ppm corresponding to the protons attached to the carbon located in the α-position relative to nitrogen. The $^1$H NMR spectrum of a mixture of **1** and HDA displays a quintet at $\delta = 2.67$ ppm for these protons (Fig. 8). This quintet arises from coupling of the α protons both to the adjacent methylene group of the alkyl chain and to the amino protons. This coupling is visible because of the coordination of the HDA ligand to the zinc atom. Similar results were obtained for OA and DDA. Integration of the signals obtained from the $^1$H NMR spectrum of the same system but with benzylamine allowed us to determine that the molecular complex has a general formula of $[Zn(Cy)_2(RNH_2)]$ (S 5). After oxidation, the $^{13}$C{$^1$H} NMR spectrum of the reaction mixture does not reveal the presence of any trace of **1** but shows peaks attributed to HDA (Fig. 9). The signals corre-

  

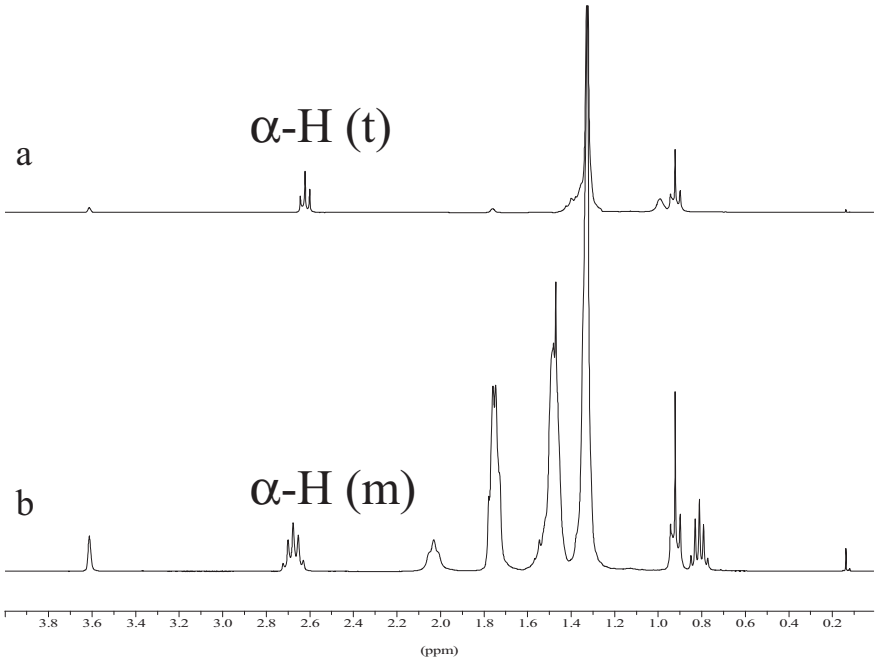


**Figure 8.** a) $^{1}$H NMR spectrum of the free DDA showing a triplet signal at $\delta = 2.62$ ppm; b) $^{1}$H NMR spectrum of the DDA ligand in the presence of **1** displaying a multiplet at $\delta = 2.67$ ppm.

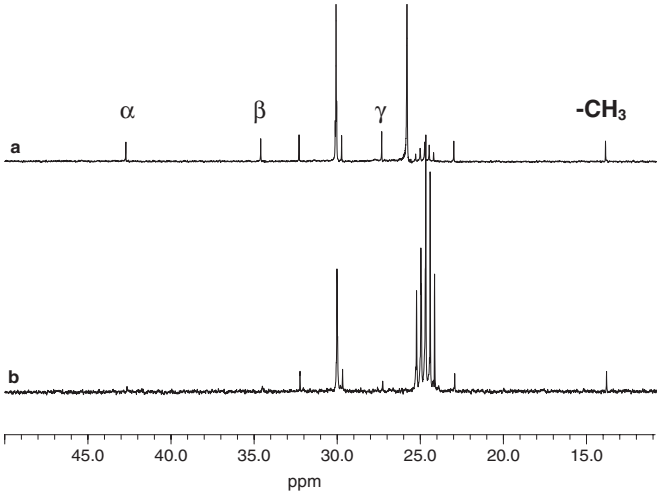


**Figure 9.** a) $^{13}C\{^{1}H\}$ NMR spectrum of the free HDA ligand and b) $^{13}C\{^{1}H\}$ NMR spectrum of the reaction mixture showing a fast exchange between free ligand molecules in solution and ligand molecules linked to ZnO through nitrogen.

sponding to the carbons in the α, β, and γ positions relative to nitrogen at $\delta = 42.69$, 34.58, and 27.31 ppm, respectively, are very broad. This phenomenon can be attributed to a fast exchange between free ligand molecules in solution and ligand molecules linked to ZnO through nitrogen. Similar results were observed when the synthesis was performed with OA or DDA (Supporting Information, Fig. S6). However, the presence of additional organic compounds was detected in the case of OA.

*2.2.6. Thermogravimetric Measurements*

Thermogravimetric analysis (TGA) measurements performed on different samples all display the same features. A first endothermic peak corresponding to the melting of the ligand is observed at a much higher temperature than for the free ligand measured under the same experimental conditions (108, 63, and 99 °C for colloids prepared using HDA, DDA, and OA as ligands, respectively, as compared to 54, 35 °C, and room temperature for the free ligands). In all nanoparticle–ligand samples a second weight loss associated with the degradation of the organic shell of the sample is then observed up to 400 °C. No endothermic peak corresponding to the evaporation of the ligand is clearly observed, whereas it is observed in the free ligands at 267, 223, and 183 °C for HDA, DDA, and OA respectively. No further weight loss is observed in the nanoparticle–ligand samples above 400 °C. The percentage of mass remaining depends on the synthetic conditions chosen. In a solvent such as THF, the percentage is around 20 % whatever the ligand, whereas the percentage is around 40 % for syntheses performed in the absence of solvent. These results illustrate that coordinating solvents, such as THF, may also be linked to the surface of the particles. More importantly, no exothermic peak at 125 °C, corresponding to $[Zn(OH)_2]$, is observed.

## 3. Discussion

The synthetic process reported in this paper involves the reaction of an organometallic precursor with moisture and air. Although the reactions of water or dioxygen with organometallic derivatives are well documented,[32] new insights into the reaction of alkylzinc complexes with dioxygen point to the possible role of this molecule in the formation of zinc oxide.[33] Indeed, the observation of cubane-like moieties by direct insertion of dioxygen molecules into the alkyl precursor observed by Lewinski et al. may also occur in our case. In order to assess the relative importance of water and dioxygen in the synthesis of the ZnO nanoparticles, specific experiments were performed in which either water or dioxygen was reacted with the molecular precursor. The first one was carried out in water-free conditions by trapping any water molecules with a column filled with $CaH_2$, whereas the second one is the reverse and was carried out under argon in the presence of degassed water vapor (see Experimental). These experiments were performed with two equivalents of OA as ligand in the absence of any other solvent. The first procedure leads to a black solid that becomes

  

ADVANCED FUNCTIONAL MATERIALS



white and luminescent when exposed to air (Coll48), while the second one leads directly to a white, luminescent precipitate (Coll49). The TEM images of Coll49 show well-defined nanorods similar to those obtained when the reaction system is exposed to moisture and air. In contrast, no well-defined particles were obtained when the reaction system was exposed only to oxygen (Supporting Information, Fig. S7). Moreover, $^{13}C\{^1H\}$ NMR spectroscopic studies allowed us to confirm the respective roles of water and dioxygen: the $^{13}C\{^1H\}$ NMR spectrum of the reaction recorded in the presence of water only shows peaks assigned to OA, whereas in addition to the peaks related to the OA ligand, the $^{13}C\{^1H\}$ NMR spectrum of the reaction performed in the presence of dioxygen shows additional peaks, close to the former OA peaks, that correspond to secondary products that may be related to a Fenton-type mechanism involving radical-oxidation reactions (Supporting Information, Fig. S7). We can therefore conclude that water vapor alone is enough to lead to the formation of zinc oxide.

It is well known that the formation of an oxide from metal cations in aqueous solution arises from a process composed schematically of two chemical reactions, namely the initial transformation of the precursor into the hydroxide and then its condensation into the oxide.[34] However, these species are in equilibrium in solution and, consequently, the hydroxide must be displaced to favor the formation of the oxide. This may occur in several ways, for example, upon heating and/or addition of a base.[9–13] On the other hand, the reaction of an organometallic complex toward oxygen or moisture is exothermic (sometimes very exothermic) and leads to an oxidized material.[32] Experimentally we do not observe any trace of hydroxide, indicating that both hydrolysis and condensation take place at room temperature. This can result either from the exothermicity of the oxidation of the organometallic precursor and/or from the presence of amines, which are bases, in solution. However, we also observe the formation of the oxide in the absence of amines. The oxidation reaction of the organometallic precursor must therefore be exothermic enough to lead to the oxide and the ligands must control the shape of the nanoparticles by kinetic control of the oxidation reaction. Our study shows that the oxidation reaction of the dicyclohexylzinc precursor with water in presence of long-alkyl-chain amine ligands can be controlled and leads to ZnO nanoparticles of well-defined shape and size, whereas in the absence of amine, agglomerated ZnO nanoparticles displaying no defined size or shape are obtained. Moreover, the stabilization by amine ligands alone is efficient enough to control the growth of the ZnO particles, in contrast with previous results reported by Cozzoli et al., who have described the formation of agglomerated or polycrystalline ZnO in a high-temperature process.[35] This demonstrates the efficiency of the method described in this paper, which allows the synthesis of crystalline nanoparticles, whose size and shape are controlled by the reaction medium, at room temperature.

As described above, a variation of the particle size with time was observed in our reactions, in agreement with previous reports.[16,36,37] In our case, after 24 h of exposure to moisture and air small particles are obtained, the size of which may double after four days depending on the solvent used. After that period no major size change is observed when the particles are kept in solution. This suggests that the size of the particles is stable after four days. Similar observations were obtained when the reaction was carried out in the presence of amine ligands only. As previously mentioned, only nanoparticles of isotropic shape are produced during the first hour of oxidation. After that period, the anisotropic growth starts, leading to nanorods whose width does not vary, although the number of long nanorods of about 120 nm increases. These observations are in agreement with a previous report on ZnO nanorods obtained by another synthetic method for which the length of the rods increased considerably with longer reaction times, whereas the width grew only slightly.[38]

The mechanism of particle formation has been well described, in particular for oxides, by Jolivet. It involves three steps, namely nucleation, growth, and ripening.[34] As already mentioned, in our case, water molecules are predominantly responsible for the formation of the ZnO particles. However, despite the precautions taken to remove any trace of water before exposure to moisture and air, some water molecules are present in the freshly distilled solvent used for the synthesis (about 50 ppm water in THF, as measured by Karl–Fisher coulumetric titration) as well as in the amine ligand, even if they are stored in a glove-box. Consequently, these water molecules could be responsible for the nucleation step by reacting with the molecular precursor and forming nuclei. Most of the precursor, however, remains intact after this step and the growth of the particles can occur when the solution is exposed to moisture and air. NMR studies have provided evidence for the ligand coordination throughout the synthesis process and have demonstrated that the amine ligands coordinated to ZnO particles are in dynamic exchange with the free ligand present in the solution. This can be directly linked to the growth of the particles observed at room temperature and in solution. In Jolivet's work, separation between the nucleation and the growth steps is reached when the precursor is in low concentration.[34] In our case, homogeneous particles are obtained when the concentration of reagent is 0.125 mol $L^{-1}$ or lower, whereas inhomogeneous particles are observed for a concentration of reagent of 0.250 mol $L^{-1}$ or above. We can therefore consider that the concentration limit for the separation of the nucleation and growth steps lies somewhere between these two values. In the third step—the ripening—the size of the particles may change even when no more zinc precursor is present in the solution. An increase of the mean size of the particles during that period is usually observed. This phenomenon corresponds to the Ostwald ripening in which the growth of the larger crystals results from the dissolution of the smaller ones. NMR observations indicate that, for the reactions performed in the presence of solvent, no more zinc precursor is present in solution after 24 h of exposition to moisture and air. The precursor is entirely consumed after 1 h when the synthesis is performed in the absence of solvent. Consequently, the evolution of size observed in solution is in agreement with an Ostwald ripening process.

It is also noticeable that nanorods are formed under certain experimental conditions. Two models are commonly used to describe the growth of particles. The first one proceeds by mass

  

transport of individual atoms. In that case, the anisotropic growth is achieved by the use of ligands to enhance the growth rate of one crystallographic face over another, as reported by Alivisatos and co-workers.[39] The second one, called "oriented attachment", introduces the coalescence of two particles to form bigger aggregates. This latter model has been reported for ZnO nanoparticles by Weller and co-workers.[40] However, the reaction conditions used by these authors differ from ours since methanol solutions containing the particles are refluxed for several hours. In our case, nanorods are formed when the synthesis is performed at room temperature in the amine ligand only, in the absence of additional solvent, whereas isotropic nanoparticles are formed at room temperature in the presence of an additional solvent. These observations suggest that the organizational ability of the ligand plays a decisive role in the shape control. Moreover, NMR studies demonstrate, for the first time, that the amine ligand is in dynamic exchange at the surface of the ZnO particles and support the hypothesis of a growth by mass transport. Interestingly, the specific-growth direction along the *c* crystallographic axis observed in the formation of the nanorods—as observed for most of the reported ZnO nanorods—corresponds to the alternate-stacking direction of the zinc and oxygen atoms. Two pathways are possible for explaining the anisotropic growth of the particles: i) the amine ligand is more labile along the *c* direction than along the others and ii) the complexation of the zinc precursor to surface oxygens is favored along this direction compared to the others. Of course, both processes may occur at the same time. Moreover, it has been reported that the wurtzite structure is highly anisotropic when the system is kinetically overdriven by an extremely high precursor concentration.[41] The same phenomenon can be observed in our case for the hexagonal zincite phase of ZnO when the synthesis is performed in the absence of solvent, for which the concentration of the precursor is a maximum.

Although the length and width of the particles have been well characterized by classical TEM measurements, questions remain concerning the third dimension of the nano-objects. Further observations performed by ultramicrotomy on elongated nanoparticles and rotation of the sample inside the electron microscope have allowed to conclude that the particles are not plates but regular nanorods. By extension of this observation we can conclude that when the growth is isotropic, nanoparticles (and not disks) of ZnO are formed. This assumption is strengthened by the values found for the half-height width (FWHM) of the *100* and *002* diffraction peaks (when the FWHM value increases, the diameter of the particle decreases). Indeed, these two peaks reflect the growth of the nanocrystal (hexagonal system) in the three dimensions. The first one is characteristic of the growth in the hexagonal-basal plane (*ab*), whereas the second one corresponds to the growth in the third dimension (*c*). If the FWHM values of these two peaks are similar, then the shape can be described as an object for which the diameter is comparable to the thickness (see Fig. 7). XRD is therefore a very powerful technique for the characterization of the shape anisotropy of the nanoparticles, as it allows the characterization of the ZnO hexagonal zincite phase and, as previously mentioned, the half-height width of the *002* peak relative to the others is indicative of the shape (isotropic nanoparticles or nanorods) of the particles. More interestingly, the low $\theta$ range also allows us to characterize the ligand used during the synthesis. The XRD pattern can hence be used as an identity card or a fingerprint of the nanoparticles, allowing us to estimate the size, shape, and also the synthetic process used for the preparation of the nano-objects.

Interestingly, all ZnO nano-objects prepared in this study can be dissolved in common organic solvents, leading to luminescent solutions (Fig. 10). This luminescence is intense enough to be directly observed by human eyes and is composed of two emission bands: one near 585 nm and the other near 370 nm, in agreement with previous reports on ZnO particles.[42,43] It is interesting to note that the two emission bands are not quenched by the solvents and that they can be observed at room temperature, both in solution and in the solid state. A complete investigation of the optical properties of these nano-objects (in solution and in the solid state) is in progress and will be published elsewhere. As can be seen in most of the TEM pictures reported here, deposition of one drop of the colloid solution onto the TEM grid leads to a monolayer of nanoparticles

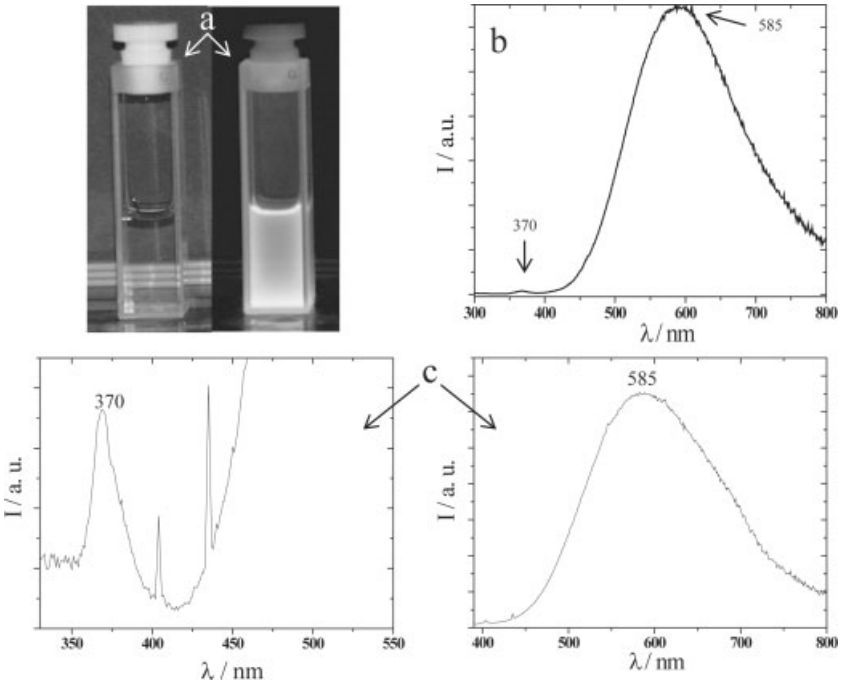


**Figure 10.** Clear and luminescent organic solutions of ZnO nanorods of about 5.8 nm × 2.7 nm prepared using the standard procedure but with a reduction of the reaction time under argon to 5 min, prior to oxidation: a) (left) in the absence of irradiation and (right) under UV irradiation ($\lambda = 312$ nm); b) in the solid state; and c) in THF (left) exciton band and (right) oxygen-vacancies band.

  

ADVANCED FUNCTIONAL MATERIALS



that tend to self-organize, although not in a two-dimensional crystalline way. Multilayers can also be obtained depending on the concentration of the solution and the number of drops deposited on the grid. The tendency of the nano-objects to self-organize onto the TEM grid is observed both for the nanoparticles and the nanorods. This organization is observed more specifically when solvents like THF, toluene, or heptane are used (see Figs. 3a,b and Figs. 5a,b and Supporting Information, Figs. S2a,b,d,e). For nanorods, this organization leads to bundles (see Fig. 5d, Fig. 6d, and Supporting Information, Fig. S7a). The SAED pattern (Fig. 6d) shows diffraction spots indicative of the alignment of the rods all along the same direction, leading to highly oriented nano-objects. However, this organizations is induced by the deposition of the nano-object onto the substrate and depends on several parameters, such as the nature of the substrate, the concentration of the colloidal solution, and the nature of the solvent.

## 4. Conclusion

We have described a one-pot, organometallic method for the synthesis, at room temperature, of ZnO nanoparticles of adjustable isotropic or rod shape that are homogeneous in both size and shape. This synthetic method uses both the very exothermic reaction of the organometallic precursor with water to produce crystalline zinc oxide and a kinetic control of the decomposition by long-alkyl-chain amine ligands in the presence or absence of additional solvents to control the size and the shape of the nanoparticles. In addition, this method is very easy to carry out and leads to quantitative yields of ZnO nanoparticles. This method may be complementary to the other methods reported so far in the literature.[4,40] It is highly versatile and allows a good control of the aspect ratio. The mechanism of particle growth involves mass transport of zinc atoms, the amine ligand playing a fundamental role in the process and remaining coordinated to the particles throughout the synthesis. It is, moreover, interesting that such semiconducting oxide nano-objects can be dissolved in common organic solvents forming clean and clear luminescent solutions that can easily be deposited on various surfaces as monolayers or thick layers, leading to new opportunities in basic research and potential applications.

## 5. Experimental

All materials were characterized using transmission electron microscopy (TEM). And X-ray diffraction (XRD); and/or selected-area electron diffraction (SAED) studies were also performed and consistently displayed the same pattern.

*Synthetic Procedures*: All reactions were performed in standard Schlenk tubes with a 14/19 opening and vacuum-line techniques. The solvents used were dried (THF over Na/benzophenone, diethyl ether over Na/benzophenone, heptane over $CaH_2$, and toluene over Na) and freshly distilled under $N_2$ prior to use, excepted for anisole, which was stored in the glove-box as received. $Zn(c\text{-}C_6H_{11})_2$ (**1**) was prepared as describe in the literature and was stored in a fridge in the glove-box[44].

*Coll1* was obtained from a THF solution (6 mL) of dicyclohexylzinc (57.9 mg, 0.25 mmol) in a Schlenk protected with an aluminum sheet. The reaction system was left for 17 h under Ar and was then exposed to moisture and air by removing the stopper. The system was left exposed to moisture and air until all the solvent had evaporated.

*Coll2, Coll3, and Coll4* were obtained following the procedure described for Coll1 but replacing THF with toluene, pentane, and diethyl ether, respectively.

*Coll5* was obtained from a solution of dicyclohexylzinc (57.9 mg, 0.25 mmol) in 6 mL of THF containing hexadecylamine (HDA; 60.4 mg, 0.25 mmol) in a Schlenk protected with an aluminum sheet. The reaction system was left for 17 h under Ar and was then exposed to moisture and air by removing the stopper. The system was left exposed to moisture and air until all the solvent had evaporated. $^{13}C\{^1H\}$ NMR (THF-$d_8$): $\delta = 42.2$ (α-C, HDA), 34.0 (β-C, HDA), 27.2 (γ-C, HDA), 13.8 ($CH_3$, HDA).

*Coll6* was obtained following the procedure described for Coll5 but replacing HDA with DDA (46.3 mg, 0.25 mmol).

*Coll7* was obtained following the procedure described for Coll5 but replacing the HDA with OA (41.3 μL, 0.25 mmol).

*Coll8* was obtained following the procedure described for Coll5 but without solvent.

*Coll9* was obtained following the procedure described for Coll6 but without solvent. $^{13}C\{^1H\}$ NMR (THF-$d_8$): $\delta = 42.5$ (α-C, DDA), 33.5 (β-C, DDA), 27.3 (γ-C, DDA), 13.8 ($CH_3$, DDA).

*Coll10* was obtained following the procedure described for Coll7 but without solvent. $^{13}C\{^1H\}$ NMR (THF-$d_8$): $\delta = 42.6$ (α-C, OA), 34.2 (β-C, OA), 27.3 (γ-C, OA), 13.8 ($CH_3$, OA).

*Coll11, Coll12, Coll13, and Coll4* were obtained following the procedure described for Coll5 but replacing THF with toluene, heptane, anisole, and diethyl ether, respectively.

*Coll15, Coll16, Coll17, and Coll18* were obtained following the procedure described for Coll6 but replacing THF with toluene, heptane, anisole, and diethyl ether, respectively.

*Coll19, Coll20, Coll21, and Coll22* were obtained following the procedure described for Coll7 but replacing THF with toluene, heptane, anisole, and diethyl ether, respectively.

*Coll23, Coll24, and Coll25* were obtained following the procedure described for Coll5 but changing the overall concentration of reagents to 0.125 mol $L^{-1}$, 0.250 mol $L^{-1}$, and 0.010 mol $L^{-1}$, respectively, which correspond to a volume of THF of 2, 1, and 12.5 mL, respectively.

*Coll26* was obtained following the procedure described for Coll9 but with two equivalents of DDA (92.6 mg, 0.50 mmol).

*Coll27* was obtained following the procedure described for Coll10 but with two equivalents of OA (82.6 μL, 0.50 mmol).

*Coll28* was obtained following the procedure described for Coll10 but with five equivalents of OA (206.5 μL, 1.25 mmol).

*Coll29* was obtained following the procedure described for Coll5 but with a reduction in the time under argon to 5 min instead of 17 h.

*Coll30* was obtained following the procedure described for Coll5 but using a stopper perforated with a small cannula, leading to a time for the oxidation/evaporation process of two weeks.

*Coll31* was obtained following the procedure described for Coll5 but the oxidation time was reduced to 24 h.

*Coll32, Coll33, and Coll34* were obtained following the procedure described for Coll31 but replacing THF with toluene, heptane, and anisole, respectively.

*Coll35* was obtained following the procedure described for Coll6 but the oxidation time was reduced to 24 h.

*Coll36, Coll37, and Coll38* were obtained following the procedure described for Coll35 but replacing the THF with toluene, heptane, and anisole, respectively.

*Coll39* was obtained following the procedure described for Coll7 but the oxidation time was reduced to 24 h.

*Coll40, Coll41, and Coll42* were obtained following the procedure described for Coll39 but replacing THF with toluene, heptane, and anisole, respectively.

*Coll43* was obtained following the procedure described for Coll10 but with two equivalents of OA (82.6 μL; 0.50 mmol) and with no incubation time.

  

*Coll44* was obtained following the procedure described for Coll27.

*Coll45* was obtained following the procedure described for Coll5 but with a constant reaction temperature of 45 °C.

*Coll46* was obtained following the procedure described for Coll45 but with a constant reaction temperature of 45 °C only during the oxidation.

*Coll47* was obtained following the procedure described for Coll8 but with a constant reaction temperature of 45 °C.

*Coll48* was obtained following the procedure described for Coll27 but the Schlenk was capped with a 20 cm column, with a 14/19 opening, filled with $CaH_2$. $^{13}C\{^1H\}$ NMR (THF-$d_8$): $\delta = 42.7$ (α-C, OA), 34.5 (β-C, OA), 27.3 (γ-C, OA), 13.8 ($CH_3$, OA).

*Coll49* was obtained following the procedure described for Coll27 but the Schlenk was then connected by a glass-connecting tube to another Schlenk containing 20 mL of distilled water that had previously been degassed by refluxing under an argon flow for 4 h.

All the synthesized nanoparticles could be redissolved in an organic solvent forming clean and clear luminescent solutions that were used to make luminescent monolayers or thicker layers of ZnO nano-objects.

*NMR Characterization*: NMR spectra were recorded in THF-$d_8$ on a Bruker DPX 300 operating at 300 MHz for $^1H$ NMR and 75 MHz for $^{13}C\{^1H\}$ NMR.

*TEM Experiments*: The TEM specimens were prepared by slow evaporation of droplets of colloidal solution of the different samples deposited on carbon-supported copper grids. The experiments were performed on a JEOL200CX operating at 200 kV.

The size distribution was determined by a numerical analysis of low-magnification TEM images. In this procedure, the different particles were identified according to an upper and lower intensity threshold and then counted and measured. Histograms of the size distribution include the measurement of at least two hundred particles and were reproduced in different regions of the samples. The size distribution was evaluated by fitting the histogram with a Gaussian curve and corresponds to its width at half-height.

*Ultramicrotomy*: Ultra-thin sections (ca. 50 nm) of ZnO nanorod samples (Coll27) were prepared using ultramicrotomy techniques. A powder sample of Coll27 was embedded into a resin Spurr R1032 matrix by heating the sample mixed with the resin precursors at 70 °C overnight. The obtained solid resin was cut into thin slices and deposited on a microscopy grid.

*X-Ray Diffraction Measurements*: The powder-diffraction patterns were obtained using a SEIFERT XRD 3000 TT X-ray diffractometer with Cu-$K\alpha$ radiation, fitted with a diffracted-beam graphite monochromator. The data were collected in the $\theta/\theta$ configuration.

*Thermogravimetric Analysis*: Thermogravimetric analysis (TGA) was performed on a SETARAM TG6DTA 92 instrument.

Received: March 18, 2004
Final version: June 9, 2004

[1] K. Westermark, H. Rensmo, H. Siegbahn, K. Keis, A. Hagfeldt, L. Ojamae, P. Persson, *J. Phys. Chem. B* **2002**, *106*, 10 108.
[2] J. A. Rodriguez, T. Jirsak, J. Dvorak, S. Sambasivan, D. Fischer, *J. Phys. Chem. B* **2000**, *104*, 319.
[3] V. Noack, H. Weller, A. Eychmüller, *J. Phys. Chem. B* **2002**, *106*, 8514.
[4] M. H. Huang, S. Mao, H. Feick, H. Yan, Y. Wu, H. Kind, E. Weber, R. Russo, P. Yang, *Science* **2001**, *292*, 1897.
[5] J. Q. Hu, Q. Li, N. B. Wong, C. S. Lee, S. T. Lee, *Chem. Mater.* **2002**, *14*, 1216.
[6] J. Y. Lao, J. Y. Huang, D. Z. Wang, Z. F. Ren, *Nano Lett.* **2003**, *3*, 235.
[7] J. Y. Lao, J. G. Wen, Z. F. Ren, *Nano Lett.* **2002**, *2*, 1287.
[8] J.-J. Wu, S.-C. Liu, *J. Phys. Chem. B* **2002**, *106*, 9546.
[9] N. S. Pesika, Z. Hu, K. J. Stebe, P. C. Searson, *J. Phys. Chem. B* **2002**, *106*, 6985.
[10] P. V. Radovanovic, N. S. Norberg, K. E. McNally, D. R. Gamelin, *J. Am. Chem. Soc.* **2002**, *124*, 15 192.
[11] E. W. Seelig, B. Tang, A. Yamilov, H. Cao, R. P. H. Chang, *Mater. Chem. Phys.* **2003**, *20*, 257.
[12] S. Bandyopadhyay, G. K. Paul, R. Roy, S. K. Sen, S. Sen, *Mater. Chem. Phys.* **2002**, *174*, 83.
[13] P. Hoyer, H. Weller, *J. Phys. Chem.* **1995**, *99*, 14 096.
[14] G. K. Paul, S. Bandyopadhyay, S. K. Sen, S. Sen, *Mater. Chem. Phys.* **2003**, *79*, 71.
[15] L. Guo, Y. L. Ji, H. Xu, P. Simon, Z. Wu, *J. Am. Chem. Soc.* **2002**, *124*, 14 864.
[16] Z. Hu, G. Oskam, R. L. Penn, N. S. Pesika, P. C. Searson, *J. Phys. Chem. B* **2003**, *107*, 3124.
[17] M. Shim, P. Guyot-Sionnest, *J. Am. Chem. Soc.* **2001**, *123*, 11 651.
[18] C. B. Murray, D. J. Norris, M. G. Bawendi, *J. Am. Chem. Soc.* **1993**, *115*, 8706.
[19] F. Dumestre, B. Chaudret, C. Amiens, M. Respaud, P. Fejes, P. Renaud, P. Zurcher, *Angew. Chem. Int. Ed.* **2003**, *42*, 5213.
[20] N. Cordente, M. Respaud, F. Senocq, M.-J. Casanove, C. Amiens, B. Chaudret, *Nano Lett.* **2001**, *1*, 565.
[21] K. Pelzer, O. Vidoni, K. Philippot, B. Chaudret, V. Collière, *Adv. Funct. Mater.* **2003**, *13*, 118.
[22] M. Gomez, K. Philippot, V. Collière, P. Lecante, G. Muller, B. Chaudret, *New J. Chem.* **2003**, *27*, 114.
[23] D. Zitoun, C. Amiens, B. Chaudret, M.-C. Fromen, P. Lecante, M.-J. Casanove, M. Respaud, *J. Phys. Chem. B* **2003**, *107*, 6997.
[24] T. Ould Ely, C. Pan, C. Amiens, B. Chaudret, F. Dassenoy, P. Lecante, M.-J. Casanove, A. Mosset, M. Respaud, J. M. Broto, *J. Phys. Chem. B* **2000**, *104*, 695.
[25] F. Dassenoy, M.-J. Casanove, P. Lecante, C. Pan, K. Philippot, B. Chaudret, *Phys. Rev. B: Condens. Matter* **2001**, *B63*, 235 407.
[26] F. Dumestre, B. Chaudret, C. Amiens, P. Renaud, P. Fejes, *Science* **2004**, *303*, 821.
[27] N. Cordente, B. Toustou, V. Collière, C. Amiens, B. Chaudret, M. Verelst, M. Respaud, J. M. Broto, *C. R. Acad. Sci., Ser. IIc: Chim* **2001**, *4*, 143.
[28] F. Rataboul, C. Nayral, M.-J. Casanove, A. Maisonnat, B. Chaudret, *J. Organomet. Chem.* **2002**, *643-644*, 311.
[29] K. Soulantica, L. Erades, M. Sauvan, F. Senocq, A. Maisonnat, B. Chaudret, *Adv. Funct. Mater.* **2003**, *13*, 553.
[30] K. Soulantica, A. Maisonnat, M.-C. Fromen, M.-J. Casanove, B. Chaudret, *Angew. Chem. Int. Ed.* **2003**, *42*, 1945.
[31] a) M. Monge, M. L. Kahn, A. Maisonnat, B. Chaudret, *Angew. Chem. Int. Ed.* **2003**, *42*, 5321. b) M. L. Kahn, M. Monge, A. Maisonnat, B. Chaudret, *French Patent CNRS, Fr 03-042825*, **2003**.
[32] J. Boersma, in *Comprehensive Organometallic Chemistry,* Vol. 2, First Edition (Ed: G. Wilkinson), Pergamon Press, Oxford, UK **1982**, p. 823.
[33] J. Lewinski, W. Marciniak, J. Lipkowski, I. Justyniak, *J. Am. Chem. Soc.* **2003**, *125*, 12 698.
[34] J.-P. Jolivet, *Metal Oxide Chemistry and Synthesis : From Solution to the Solid State*, John Wiley and Sons, Chichester, UK **2000**.
[35] D. P. Cozzoli, L. M. Curri, A. Agostiano, G. Leo, M. Lomascolo, *J. Phys. Chem. B* **2003**, *107*, 4756.
[36] A. van Dijken, E. A. Meulenhkamp, D. Vanmaekelbergh, A. Meijerink, *J. Phys. Chem. B* **2000**, *104*, 1715.
[37] Z. Hu, G. Oskam, P. C. Searson, *J. Colloid Interface Sci.* **2003**, *263*, 454.
[38] O. Harnack, C. Pacholski, H. Weller, A. Yasuda, J. M. Wessels, *Nano Lett.* **2003**, *3*, 1097.
[39] L. Manna, E. C. Scher, A. P. Alivisatos, *J. Am. Chem. Soc.* **2000**, *122*, 12 700.
[40] C. Pacholski, A. Kornowski, H. Weller, *Angew. Chem. Int. Ed.* **2002**, *41*, 1188.
[41] X. Peng, L. Manna, W. Yang, J. Wickham, E. Scher, A. Kadavanich, A. P. Alivisatos, *Nature* **2000**, *404*, 59.
[42] A. van Dijken, E. A. Meulenhkamp, D. Vanmaekelbergh, A. Meijerink, *J. Lumin.* **2000**, *90*, 123.
[43] P. Yang, H. Yan, S. Mao, R. Russo, J. Johnson, R. Saykally, N. Morris, J. Pham, R. He, H.-J. Choi, *Adv. Funct. Mater.* **2002**, *12*, 323.
[44] K.-H. Thiele, S. Wilcke, M. Ehrhardt, *J. Organomet. Chem.* **1968**, *14*, 13.

  